

# Active Control for Statistically Stationary Turbulent Premixed Flame Simulations

J. B. Bell, M. S. Day, J. F. Grcar, M. J. Lijewski

Lawrence Berkeley National Laboratory  
Mail Stop 50A-1148  
1 Cyclotron Road  
Berkeley, CA 94720-8142 USA  
e-mail: jbbell@lbl.gov

## Abstract

The speed of propagation of a premixed turbulent flame correlates with the intensity of the turbulence encountered by the flame. One consequence of this property is that premixed flames in both laboratory experiments and practical combustors require some type of stabilization mechanism to prevent blow-off and flashback. The stabilization devices often introduce a level of geometric complexity that is prohibitive for detailed computational studies of turbulent flame dynamics. Furthermore, the stabilization introduces additional fluid mechanical complexity into the overall combustion process that can complicate the analysis of fundamental flame properties. To circumvent these difficulties we introduce a feedback control algorithm that allows us to computationally stabilize a turbulent premixed flame in a simple geometric configuration. For the simulations, we specify turbulent inflow conditions and dynamically adjust the integrated fueling rate to control the mean location of the flame in the domain. We outline the numerical procedure, and illustrate the behavior of the control algorithm on methane flames at various equivalence ratios in two dimensions. The simulation data are used to study the local variation in the speed of propagation due to flame surface curvature.

## Contents

<b>1</b>	<b>Introduction</b>	<b>3</b>
<b>2</b>	<b>Computational Methodology</b>	<b>4</b>
2.1	Simulation Methodology . . . . .	4
2.2	Flow Configuration . . . . .	5
2.3	Control Methodology . . . . .	5
2.4	Determination of Control Parameters . . . . .	6
<b>3</b>	<b>Controlled Methane Flames</b>	<b>8</b>
3.1	2-step Mechanism . . . . .	8
3.2	GRI-Mech 3.0 Mechanism . . . . .	10
<b>4</b>	<b>Analysis of the GRI-Mech 3.0 Flames</b>	<b>11</b>
4.1	Appearance of the Flames . . . . .	11
4.2	Global Turbulent Burning Speed . . . . .	14
4.3	Local Burning Speed Behavior . . . . .	16
<b>5</b>	<b>Conclusions</b>	<b>20</b>
	<b>Acknowledgements</b>	<b>21</b>
	<b>References</b>	<b>21</b>
	<b>Figures</b>	<b>25</b>

## 1 Introduction

A well-known property of turbulent premixed flames is that their speed of propagation correlates to the turbulent intensity in the unburned mixture. See Bradley [5] and Peters [28] for a discussion of this issue. As a consequence, premixed flames are inherently unstable when propagating against a turbulent flow whose intensity increases upstream but decays downstream. To have a stable flame for either laboratory analysis or for a practical combustor requires some type of flame stabilization mechanism. A variety of approaches are used to stabilize premixed turbulent flames in the laboratory [10]. For example, the Twenty-Ninth Combustion Symposium includes studies by Sattler et al. [33] of a turbulent V-flame, Shepherd et al. [34] of a swirl-stabilized flame, Most et al. [24] of a bluff-body stabilized flame, and Chen et al. [9] of Bunsen and stagnation flames. These stabilization mechanisms are necessary to control the flame location so that data can be collected. Each stabilization mechanism has advantages and disadvantages. Bluff-body stabilized flames, V-flames and Bunsen flames are fluid-mechanically fairly simple but there is substantial flow tangential to the flame and the flame encounters different levels of turbulence further from the burner nozzle. The low-swirl geometry produces a statistically nearly flat flame but the fluid mechanics of the stabilization are quite complex. Stagnation plate flames are geometrically and fluid mechanically simple but the flame experiences a substantial mean strain and heat loss to the plate. In each case, the additional complexity introduced by the stabilization complicates both the analysis of the flame data and the implication of the results to the characterization of premixed turbulent flames.

For the most part, computational studies of premixed flames that include detailed chemistry and transport and resolve the relevant fluid-mechanical scales have not included any of these stabilization mechanisms. For an exception, see the model of a three-dimensional (3D) turbulent V-flame by Bell et al. [4]. The computational demands of these types of simulations combined with the specialized numerical algorithms typically used for direct numerical simulations make including physical stabilization mechanisms prohibitively expensive.

The idealized configuration that we use for the present study is a modified version of one used frequently in the numerical study of premixed turbulent flames. A flat steady laminar premixed flame is initialized in a computational domain and allowed to propagate toward a boundary where turbulent perturbations have been superimposed on a mean inflow. After the turbulence interacts with the flame for a sufficient period of time, statistics are gathered from the solution to quantify the extent to which the turbulent fluctuations modify the flame structure. There is an extensive literature on computational studies of this type in 2D, both with simplified and detailed chemistry. Examples germane this configuration include Baum et al. [2] who studied turbulent flame interactions for detailed hydrogen chemistry, and Haworth et al. [19] who examined the effect of inhomogeneous reactants for propane–air flames using detailed propane

chemistry. Analogous studies in 3D have been performed by Rutland and Trouvé [32], Trouvé and Poinso [38], Zhang and Rutland [41], and Chakraborty and Cant [7]. All of these 3D studies were based on simplified chemistry. More recently Tanahashi et al. [36,37] have performed simulations of this type for turbulent premixed hydrogen flames with detailed hydrogen chemistry. Bell et al. [3] performed a similar study for a turbulent methane flame.

Computational studies involving the idealized flow configuration suffer from a fundamental instability that prevents stabilization of the computed flames. If the flame begins to propagate faster than the specified inflow velocity, then the flame migrates upstream nearer the stronger turbulence which further increases its speed. Similarly, a propagation speed slower than the inflow velocity causes the flame to migrate downstream into further decayed turbulence where the flame propagation is even slower. Thus the flame may not encounter a given turbulence intensity long enough to gather statistics about its behavior at that intensity. Moreover, since the flame is not statistically stationary in the computational domain, it will often migrate to either the domain inflow or outflow boundary, terminating the simulation.

In this paper, we apply a feedback control algorithm to automatically adjust the inflow velocity to stabilize flames in the idealized configuration. The control algorithm allows long-time simulation of statistically stationary flames in a configuration free of complications associated with physical boundary conditions. In the next section, we briefly describe the basic simulation methodology for low-speed reacting flows, and describe the feedback control procedure. We then demonstrate the ability of the algorithm to stabilize premixed methane flames in 2D. We next demonstrate the utility of this algorithm by exploring global burning statistics and correlations in localized burning with flame geometry.

## 2 Computational Methodology

### 2.1 Simulation Methodology

The simulations presented here are based on a low Mach number formulation of the reacting flow equations. The methodology treats the fluid as a mixture of perfect gases. We use a mixture-averaged model for differential species diffusion and ignore Soret, Dufour, gravity and radiative transport processes. Unless explicitly stated otherwise, the chemical kinetics are modeled using the GRI-Mech 3.0 methane mechanism [15, 35] with 53 species and 325 fundamental reactions. The basic discretization combines a symmetric operator-split coupling of chemistry and diffusion processes with a density-weighted approximate projection method. The projection method incorporates the constraint on the velocity divergence that arises in the low Mach number formulation. The resulting integration of the advective terms proceeds on the time scale of the relatively slow advective transport. Faster diffusion and chemistry processes are treated time-implicitly. This integration scheme is embedded in a parallel adaptive mesh

refinement algorithm framework based on a hierarchical system of rectangular grid patches. The complete integration algorithm is second-order accurate in space and time, and discretely conserves species mass and enthalpy. The reader is referred to [13] for details of the low Mach number model and its numerical implementation and to [3] for previous applications of this methodology to the simulation of premixed turbulent flames.

## 2.2 Flow Configuration

The flow configuration we consider initializes a flat laminar flame in a domain oriented so that the flame propagates downward. Since there is no gravitational force included, up and down are for orientation only. A cold fuel-air premixture enters the domain through bottom boundary, and hot combustion products exit the domain through the top. The remaining computational boundaries are periodic. Along the inflow face we specify both a mean inflow velocity and turbulent fluctuations that are superimposed on the mean inflow. A control algorithm is used to adjust the mean inflow rate to hold the flame in the domain indefinitely. As a result, the calculation essentially is carried out in a Lagrangian frame, moving with the intrinsic mean speed of the flame for a particular fuel, stoichiometry, and turbulence intensity. The following section details the strategy for computing the mean inflow rate needed to hold the flame statistically steady in the simulation domain.

## 2.3 Control Methodology

Because the inflowing fuel velocity will contain significant fluctuations, the resulting flame surface will be wrinkled. We will develop a simplified model to describe the flame dynamics in 1D, and then develop the control algorithm for the multidimensional flame in the context of that simplified model. The mean vertical flame location,  $h(t)$ , is computed from the evolving 2D solution by integrating the instantaneous mass of fuel in the domain and dividing this result by the product of the fuel density and inlet area at the inflow boundary. This averaged flame location propagates downward at some effective turbulent flame speed,  $s$ , relative to the mean fluid motion. The control problem is to specify a mean inflow velocity  $v_{\text{in}}(t)$  that automatically pushes the flame from an initial flame location,  $h(0) = \alpha$ , to the target flame location,  $h(t) = \beta$ .

The dynamics of the average flame position can be modeled using a stochastic differential equation of the form

$$dh = (v_{\text{in}}(t) - s(h))dt + d\omega \quad (1)$$

where the effective flame speed,  $s(h(t))$  is a function of the time-dependent flame position, and must be estimated as part of the control process. The final term,  $d\omega$ , represents high-frequency fluctuations in the turbulent flame speed due to stochastic fluctuations in the inflow stream.

Given a quadratic cost functional associated with equation (1) and assumptions about the noise term, there are well-known procedures for deriving optimal control strategies: see Kushner [23], Caines [6] and Chen, Chen and Hsu [8]. However, in the present case, we do not have a closed-form characterization of the fluctuations. Further, since the control velocity,  $v_{\text{in}}(t)$ , determines the boundary condition for the low Mach number solver, we need to impose additional constraints on the profile. In particular, we need  $v_{\text{in}}(t)$  to be smooth in time and we need to impose limits on how much it can change during a time step. These heuristic constraints are chosen so that we do not introduce instabilities or inaccuracies into the simulation algorithm or subject the flame to large accelerations that could induce spurious fluid dynamical behavior from Rayleigh-Taylor instabilities.

We take  $v_{\text{in}}(t)$  to be piecewise linear and limited such that the inflow velocity cannot change dramatically during a time step. These smoothness criteria constrain how rapidly  $v_{\text{in}}$  can respond to changes in  $h$  and to noise. Consequently, we need to introduce a time scale,  $\tau$ , which is the target lag for reaching the control state. We want to estimate  $\Delta v$ , the change in  $v$  from time  $t_0$  to  $t_0 + \tau$ , so that  $h$  reaches  $\beta$  over the period  $\tau$ . We assume that  $\tau$  is sufficiently large that the noise  $d\omega$  has mean zero over the interval  $[t, t + \tau]$ , yet assume that the turbulent flame speed,  $s$ , is slowly varying. If we are given  $h(t_0)$ ,  $v_{\text{in}}(t_0)$ , and an estimate  $s_{\text{est}}$  of the mean flame speed over the interval, then assuming  $\Delta v$  is constant, we can integrate equation (1) to obtain:

$$\beta = h(t_0) + \tau(v_{\text{in}}(t_0) - s_{\text{est}}) + \frac{\tau^2}{2}\Delta v$$

For the purposes of computing this integral, we estimate  $s_{\text{est}}$  from the change in fuel mass in the domain during the previous time step. To enforce the smoothness required by the flow solver we then limit  $\Delta v$  so that over a time step the velocity does not change by more than  $0.1 \max\{v_{\text{in}}(t_0), v_{\text{min}}\}$  where  $v_{\text{min}}$  is a minimum velocity scale of the problem that can be computed from the post-flame velocity of the laminar flame propagating into fluid at rest. Also, we find our simulation methodology to be more robust if we avoid large outflows at the inflow boundary by requiring  $v_{\text{in}} \geq 0$ . Note that this strategy therefore relies on burning to move the flame in the upstream direction.

## 2.4 Determination of Control Parameters

Robustness of this control algorithm depends strongly on the heuristic parameters. In order to explore the implications of these parameters, we perform synthetic tests of the algorithm with parameters chosen to reflect conditions of a typical flame simulation, including a simple model for  $s$ . A wealth of compiled experimental data suggests that the effective propagation speed of a turbulent premixed flame correlates with the intensity of the turbulence. We expect, therefore, that the closer the flame is to the inlet boundary (turbulence source) the

faster it will propagate. In our configuration, this suggests that  $s'(h) < 0$ . For our model, we set

$$s(h) = \bar{s}(1 - \gamma(h - \beta))$$

so that  $s'(h) = -\gamma\bar{s}$ . For our tests, we take the remaining parameters to reflect values corresponding to a lean premixed methane flame:  $\bar{s} = 0.3$ ,  $\gamma = 0.1$ ,  $\beta = 0.005$ ,  $\alpha = 0.001$  and  $\Delta t = 0.00002$ . This  $\Delta t$  is typical of timestep sizes found on the coarsest meshes in our adaptive mesh refinement algorithm for low Mach number flows; we refine in both space and time so the finer, refined meshes have proportionately smaller time steps. To simulate noise due to the turbulent fluctuations, we used uniformly distributed random perturbations of  $\pm 33\%$ .

Simulation results showing the “flame location,”  $h$ , and control velocity computed by the algorithm for various values of  $\tau$  are shown in Figures 1 and 2, respectively. From the results, if  $\tau$  is too small, corresponding to quickly controlling the flame, then the restrictions on changing the velocity lead to fluctuations

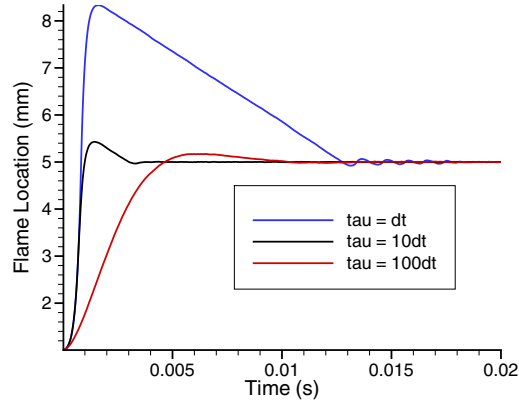


Figure 1: *Synthetic flame control simulations – flame location.*

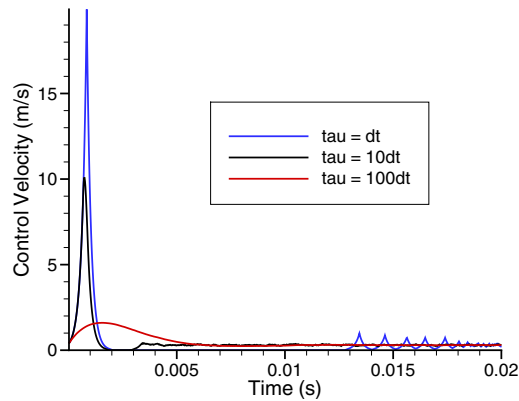


Figure 2: *Synthetic flame control simulations – control velocity.*

on the synthetic flame location that persist for considerable time. If  $\tau$  is too large, the system is well-behaved but a relatively long time is required to reach the desired state. Our test indicate that  $\tau = 10\Delta t$  appears to provide a robust control that relatively rapidly controls the flame to the desired location. We note that even if the control is started at the correct location and correct velocity, setting  $\tau = \Delta t$  does not provide satisfactory results. The interplay of perturbations from the noise and the restrictions on changing  $v_{\text{in}}$  lead to fairly large oscillations as indicated in Figure 3.

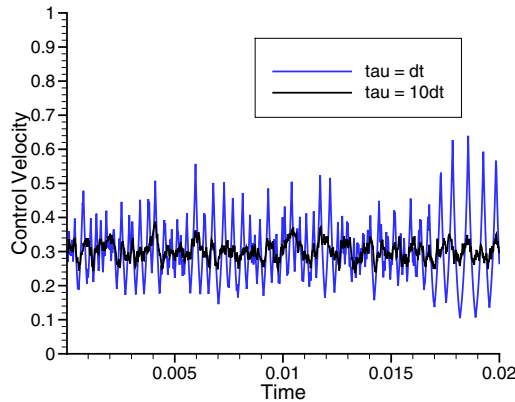


Figure 3: *Synthetic flame control simulations starting from correct flame location and speed.*

### 3 Controlled Methane Flames

#### 3.1 2-step Mechanism

We validate the control algorithm using a representative time-dependent simulation of premixed methane combustion. A simplified combustion model reduces the cost of integration so that the control algorithm can be observed over a long time period in order fully characterize the resulting performance and system response. This simplified calculation assumes a unity Lewis number [29] for transport and it has just 6 chemical species:  $\text{CH}_4$ ,  $\text{O}_2$ ,  $\text{CO}_2$ ,  $\text{H}_2\text{O}$ ,  $\text{CO}$ ,  $\text{N}_2$ . The 2-step kinetics mechanism (see [26], Model “2”, with Arrhenius rates given by [14, 40, 42]) incorporates a global reaction step for methane oxidation, and a reversible reaction to convert  $\text{CO}$  to  $\text{CO}_2$  in the product stream. The fuel equivalence ratio of the methane-air mixture is  $\phi = 1$ . For additional computational convenience here, the flame chemistry and transport were modified to artificially thicken the flame to  $\delta_L = 0.7$  mm, and to adjust its propagation speed to  $s_L = 36$  cm/s. These values approximately match those of the corresponding laminar flame computed with a more detailed transport model and the GRI-Mech 3.0 [15, 35] mechanism. The modifications were accomplished



by uniformly increasing all transport coefficients by a factor of 2, and reducing chemical production rates uniformly by a factor of 3, following ideas discussed in [12].

The time-dependent calculation is performed using the flame sheet configuration discussed above. Flow enters a 2D domain through the bottom boundary, proceeds upward through a dynamically wrinkling flame surface, and exits the top outflow boundary. The side walls are periodic. The length of the inlet face  $L = 28.6 \delta_L$ , and the height of the domain  $H = 2L$ . The fluctuations are generated in an auxiliary calculation prior to the controlled flame simulation. A random velocity field is generated on a  $L \times L$  domain with an energy spectrum of the form

$$E(k) = \frac{\left(\frac{k}{k_i}\right)^4}{\left[1 + \left(\frac{k}{k_i}\right)^2\right]^{\frac{17}{6}}} \exp\left[-\frac{9}{4} \left(\frac{k}{k_d}\right)^{\frac{4}{3}}\right]$$

where  $k$  is the wavenumber,  $k_d = 1/(2\Delta x)$ , and  $k_i$  is the peak frequency, which is adjusted empirically to give the desired integral scale. This form is characteristic of 2D decaying isotropic turbulence [21]. Rather than using the random field directly, we first evolve it for several eddy turnover times using an incompressible Navier-Stokes solver [1] at resolution comparable to the finest meshes in the reacting flow simulations to ensure that the phases are realistic (see below). To accommodate this evolution the initial field is generated at a somewhat higher turbulence intensity and the incompressible evolution is continued until the turbulent intensity reaches the desired level. The resulting fluctuations have an effective integral scale length  $\ell_t \sim 2.6 \delta_L^T$  and turbulent intensity  $u' \sim 1.7s_L$ . They are added to a mean vertical flow given dynamically by the feedback control algorithm to model the advection of turbulence through the inflow boundary. By cycling through the periodic fluctuation data, this technique provides an endless source of fluctuations with a periodicity length  $L$ . The amount of corresponding time for cycling through the data is dependent on the (time-dependent) control velocity. The system is on the boundary between the corrugated and distributed flamelet regime [28], but also very nearly laminar.

The simulation is carried out with a three-level adaptive grid hierarchy. The refinement criteria is such that the flame surface remains resolved with a uniform grid spacing at the finest level of  $\Delta x = 39 \mu\text{m}$ . The base grid covering the entire domain is a factor of four coarser, and an intermediate level a factor of two finer than the base grid is used to resolve the turbulent fluctuations between the inlet boundary and the flame surface.

A steady solution obtained from the PREMIX code [22] and the identical transport and chemistry models is used to initialize a flat flame parallel to the inlet face. The flame position is initially below the target height of  $\beta = 5 \text{ mm}$  above the inlet boundary. The flame is evolved using the control algorithm to automatically adjust the inflow rate.

Figure 4 shows the flame location and control velocity as a function of time over approximately 75 integral-scale eddy turnover periods,  $\tau_t = \ell_t/u' \approx 1.8 \text{ ms}$ . The initial transient indicates that the control quickly increases the inflow rate

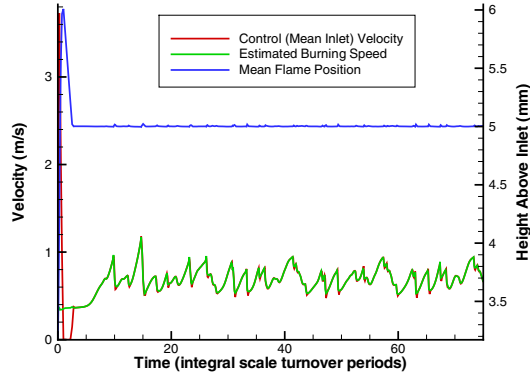


Figure 4: *Performance of control algorithm for  $\phi = 1.0$  case with simplified chemistry.*

to shift the flame upward. The flame overshoots the target so the inflow velocity is adjusted automatically to zero for a short time interval. After the flame burns back upstream to the set point, both the control and the burning speed briefly settle into a value, about 38 cm/s, that is near the speed of a flat laminar flame. During this initial phase the inflowing mixture is carrying decaying turbulence toward the flame, which is only slightly wrinkled. At approximately 10 ms, the fluctuations begin to wrinkle the flame causing a dramatic increase in flame surface area and a corresponding increase in the burning speed. The control algorithm increases the inflow rate in response to flame surface area perturbations so as to maintain a constant volume of unburned mixture. Note that the large periodic transients in fuel consumption correspond to flame topology changes such as localized necking and pinching off of flame fragments, but that the volume of unburned mixture is steady as indicated by the nearly constant mean flame position.

This example demonstrates that for atmospheric stoichiometric premixed methane flames in this corrugated flamelet regime, our control algorithm is sufficiently robust to stabilize the flame in the computational domain, allowing the collection of detailed flame statistics. In Figure 4, we observe that after the initial transients, the flame speed exhibits a cyclic repetition with a period of approximately  $17 \tau_t$ , corresponding to the time to traverse the auxiliary file of turbulent fluctuations. With our current approach for introducing turbulent fluctuations, the size of the auxiliary fluctuation file effectively places an upper bound on the scales of temporal dynamics that are representable.

### 3.2 GRI-Mech 3.0 Mechanism

We now apply the control methodology described above to a series of methane flames modeled in significantly greater detail, using the GRI-Mech 3.0 chemistry mechanism (53 species, 325 reactions) and a mixture-averaged diffusive transport

model. Three flames are chosen to highlight variations observed in a methane flame’s response to flowfield flame surface curvature (see, for example, Tseng et al. [39]). The three cases have stoichiometries,  $\phi = 0.55, 0.75, 1.0$ . Table 1 lists various properties of the corresponding steady laminar one-dimensional flame solutions computed using the PREMIX [22] code. As before, the computational domain in all three cases is periodic in the horizontal direction with inflow on the bottom face and outflow at the top. In all three cases, the computational domains have dimensions  $L \times H = 46 \delta_L^T \times 92 \delta_L^T$ . The fluctuations in the inflow stream were generated for each case separately using a process identical to that discussed in the first example. The resulting fluctuations had an effective integral scale length  $\ell_t \sim 2.6\delta_L^T$  and turbulent intensity  $u' \sim 1.7s_L$ , measured with respect to the properties of each flame.

Table 1: *Characteristics of the three laminar methane-air flames of different stoichiometries at 1 atmosphere. Thermal flame thickness is calculated as the change in temperature through the flame divided by the maximum temperature gradient,  $\delta = (T_{\max} - T_{\min}) / \max \|\nabla T\|$ .*

fuel equiv- alence ratio $\phi$	thermal flame thickness $\delta$ ( $\mu\text{m}$ )	flame speed $s_L$ (cm / s)	fuel consum- ption rate (g / cm s)	isotherm of peak heat release (K)	peak local fuel consumption (mg / mL s)
1.00	433	36.2	0.2380	1684	134
0.75	584	22.34	0.1070	1516	51.3
0.55	1313	7.62	0.0273	1379	7.03

Adaptive mesh refinement was used in all the simulations to maintain approximately 22 uniform grid cells across the thermal width of the flames throughout their evolution. Dynamic refinement for these simulations was based on the magnitude of vorticity and on a flame marker,  $\text{CH}_3$ . In each case, we waited until the flame height stabilized before collecting the statistical analysis data. The time-dependent data represents snapshots of the three cases taken at uniform intervals over approximately five  $\tau_t$ .

## 4 Analysis of the GRI-Mech 3.0 Flames

### 4.1 Appearance of the Flames

Representative snapshots of the temperature fields are shown in Figure 5. The three flames of different stoichiometries appear qualitatively similar, as expected given that the flames are at the same point on the regime diagram for premixed turbulent combustion, the so-called Borghi diagram [27]. At any instant in time, the flame surface shows the characteristic wrinkling expected of a turbulent

premixed flame, namely, regions where the flame is smoothly bowed toward the reactants separated by sharper cusps protruding into the burned region. Since the bows are the larger geometric feature, they consume more of the unburned mixture whose amount in the domain is kept constant by the control. Thus the bows are relatively stable in the frame of reference of the computational domain. The behavior at the cusps is more dynamic. Cusps are observed to periodically grow into elongated channels after which there is period of apparent rapid movement when the sides of the channel close upon each other and the cusp returns to a more typical position relative to the rest of the flame. Occasionally in this process, a channel will burn through in its center detaching a bubble of unburned fuel surrounded by products. An example of this is shown in the snapshot of the  $\phi = 1$  flame in Figure 5 where an elongated channel extends through the periodic boundary. Here, the unburned mixture at the cusp is about to detach. Extinction, marked by dramatic and sudden reductions in fuel consumption along the flame surface, was not observed in any of the cases.

We examine the distribution of the curvature of the flame over the course of the simulation to quantitatively demonstrate the similarity of the flames. As indicated in Table 1, we associate the location of the flame with a particular isotherm. The vector field of unit normals to all the isotherms throughout the domain can be calculated as a  $\hat{n} = -\nabla T / \|\nabla T\|$  using centered differences on the underlying uniform, rectangular meshes. Note these normals have been chosen to point toward the cold, unburned mixture. The curvature of the isotherms is then  $\kappa = \nabla \cdot \hat{n}$  again evaluated throughout the domain using centered differences. We then interpolate this  $\kappa$  to the isotherm corresponding to the peak heat release

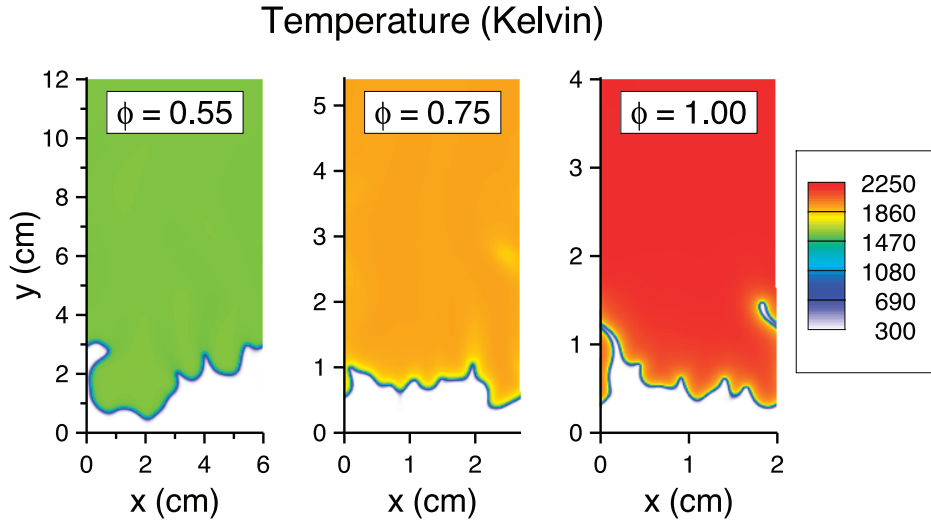


Figure 5: *Temperature in the three flames.*

from the laminar flame solution, which we use as the operational definition of the flame surface. With this definition, the curvature is negative at cusps and positive in the bowed regions.

When the curvature is scaled to the laminar flame thermal thickness, the probability density functions (PDFs) of curvature for all three flames are coincident, indicating that all three flames are experiencing the same degree of wrinkling. See Figure 6. These curves are the probability of finding a portion of flame with the given value of curvature while the flame evolves through several hundred time steps (spanning at least five eddy turnover periods) once reaching a statistically stationary state. We note that the distributions peak slightly to the positive side of zero. In general there is a greater probability of finding positive curvature (the bowed regions), but at high curvature the distributions show a strong bias toward negative values (the cusps). This skewness, emphasized here by the choice a log scale on the ordinate, is typical of turbulent flames, as noted above. Finally, we note that a nontrivial fraction of the flame surface is subject to curvature that is not “small.”

These flame dynamics are all consistent with the regime diagram’s characterization of these flames as being in the flamelet regime. Flames in the corrugated and wrinkled flamelet regimes tend to maintain a well-defined flame front structure with nearly parallel isocontours of species and temperature. A detailed attempt to base the regime diagram on observations of 2D direct numerical simulations was carried out by Poinot, Veynante, and Candel [30] using interactions between flames and single vortex pairs. Their work could be successfully

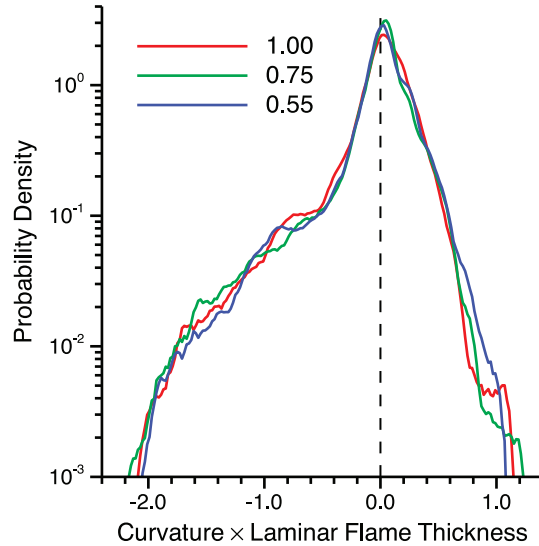


Figure 6: *Probability density of curvature scaled by laminar flame thickness for the three flames of different stoichiometries. Density is calculated by a moving average over 5 intervals of width 0.02 (nondimensional) on the horizontal axis.*

extended to long-duration observations of flames in more complicated, stochastic flow fields using the control strategy developed here.

## 4.2 Global Turbulent Burning Speed

For the initial analysis of the results, we look first at the effective turbulent flame speed  $S_c^G$ , defined in terms of the integrated fuel consumption

$$S_c^G = \frac{1}{A_L (\rho Y_{\text{CH}_4})_{\text{in}}} \int_{\Omega} \rho \omega_{\text{CH}_4} d\Omega$$

where  $A_L$  is the area of the flat laminar flame (ie, the width of the domain,  $L$ ),  $(\rho Y_{\text{CH}_4})_{\text{in}}$  is the inflowing methane mass density and  $\rho \omega_{\text{CH}_4}$  is the rate of methane mass consumption. In Figure 7 we plot  $S_c^G$ , normalized by  $S_L$ , versus time, normalized by  $\tau_t$ , for each case. In these figures, the dramatic drops in turbulent speed correspond to rapid flame area loss at the burning of long thin channels, and to the rapid consumption of detached pockets of unburnt material. The plot demonstrates a large (20–50%) variability in the instantaneous turbulent flame speeds for all cases. When examined at the length and time scales representative of the computation, it makes little sense to talk about turbulent flame speed as a single number. More revealing data may be the PDFs of turbulent flame speed shown in Figure 8. These PDFs are centered at 200–250% of  $S_L$ , and are quite broad. The  $\phi = 0.75$  case appears bimodal; however, it is not clear if this is a real effect or evidence of a lack of adequate statistics.

We now explore the relationship between aggregate fuel consumption rate and the flame area resulting from wrinkling due to the inflow fluctuations. Figure 9 shows a scatter plot of  $S_c^G$  versus the instantaneous flame area  $A^G$  (or, length of isotherm contour we associated with the flame surface at that instant in time). The symbols represent data from solutions taken at uniform intervals throughout the sample period. To a very good approximation, the fuel

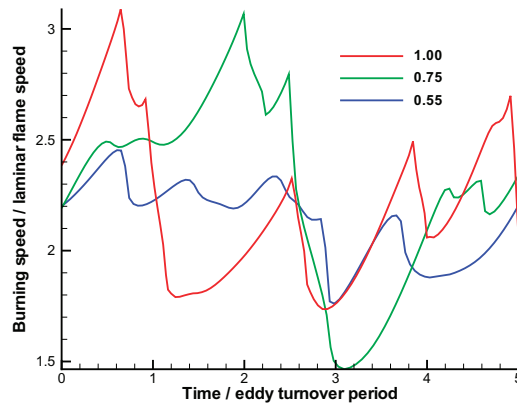


Figure 7: *Turbulent flame speed for the three flames.*

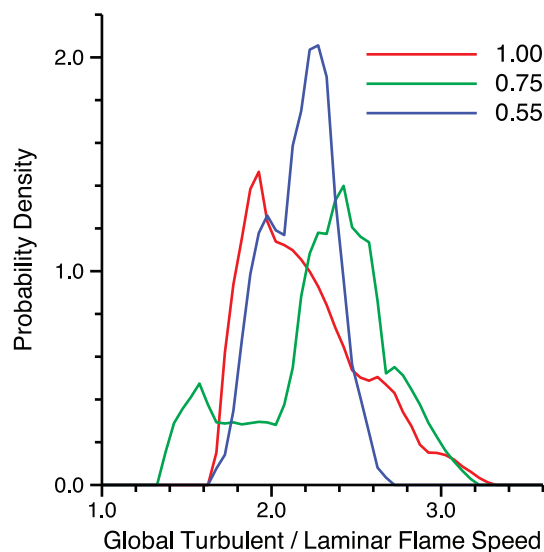


Figure 8: *Probability density of overall turbulent speedup for the three flames of different stoichiometries. Density is calculated by a moving average over 5 intervals of width 0.05 (nondimensional) on the horizontal axis.*

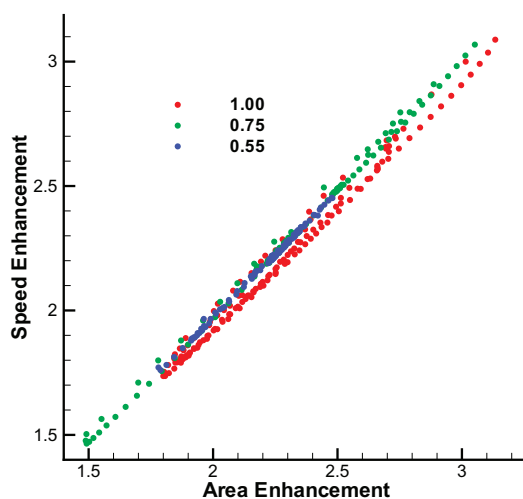


Figure 9: *Turbulent flame speed versus flame area.*

consumption rate in the domain scales with the overall area of the flame for all three stoichiometries. Thus, at least on average, the turbulent flame speed is directly proportional to the flame area, even across the large excursions in turbulent flame speed. Note that the stoichiometric flame is slightly slower than predicted by its area and the laminar flame speed. This reflects associated

changes in Markstein number with  $\phi$ , which are discussed in more detail in the next section.

### 4.3 Local Burning Speed Behavior

In this section, we look at the local flame behavior in more detail. To refine the analysis of flame speed we look at the variation in fuel consumption along the flame surface for each of the three cases. Figure 10 shows representative samples for each flame with a blow up of a localized region of high curvature. For the  $\phi = 1.0$  flame, we see a dramatic enhancement in fuel consumption at the cusps, which corresponds to a region of large negative curvature. We observe a comparable reduction in fuel consumption in regions of large positive curvature. Similar but less pronounced behavior is observed for  $\phi = 0.75$ ; however, for  $\phi = 0.55$  the observed trends reverse with higher fuel consumption in regions of positive curvature and lower fuel consumption in regions of negative curvature.

We would like to relate this change in the behavior of the fuel consumption to the behavior of the local flame speed. There are several potential definitions of local flame speed; see, e.g., Poinso and Veynante [29] for a discussion of possible choices. Here we will define a local flame speed based on integrated local fuel consumption in the following way. To define the integrals we will define local coordinates near the flame using arclength along the flame and a normal coordinate defined in terms of a progress variable,  $c$ , defined such that  $c = 0$  in the unburned reactants, and  $c = 1$  in the products. The progress variable may be based on any scalar variable that is monotonic across the flame surface; here, we will use normalized temperature to define the progress variable.

At uniform intervals along the flame, we extend local normals by following integral curves of the gradient of  $c$  toward both the products and fuel. These normals define a series of adjacent disjoint wedge-shaped volumes,  $\Omega$ , surrounding the flame, and extending well beyond the region of high chemical reactivity. A local burning speed may then be defined over each of these volume:

$$S_c^\ell = \frac{1}{A^\ell (\rho Y_{\text{CH}_4})_{\text{in}}} \int_{\Omega} \rho \omega_{\text{CH}_4} d\Omega \quad (2)$$

where  $A^\ell$  is the area (length) of the intersection of  $\Omega$  with the flame. A typical example of a set of such normals, and the resulting wedge-shaped volumes is depicted in Figure 11. The example is taken from the  $\phi = 1.0$  case, and includes the instantaneous advection streamlines superimposed for reference. Defining the local speed in this way has the property that the turbulent burning speed is its area-weighted average:

$$S_c^G = \sum_{i=1}^{N_{\text{wedges}}} S_c^{\ell,i} \frac{A^{\ell,i}}{A^G}.$$

where  $N_{\text{wedges}}$  is the number of discrete wedge-shaped volumes tiling the entire flame surface. In addition to preserving the total integral of fuel consumption,



## Ratio of Local Fuel Consumption to Peak Laminar Value

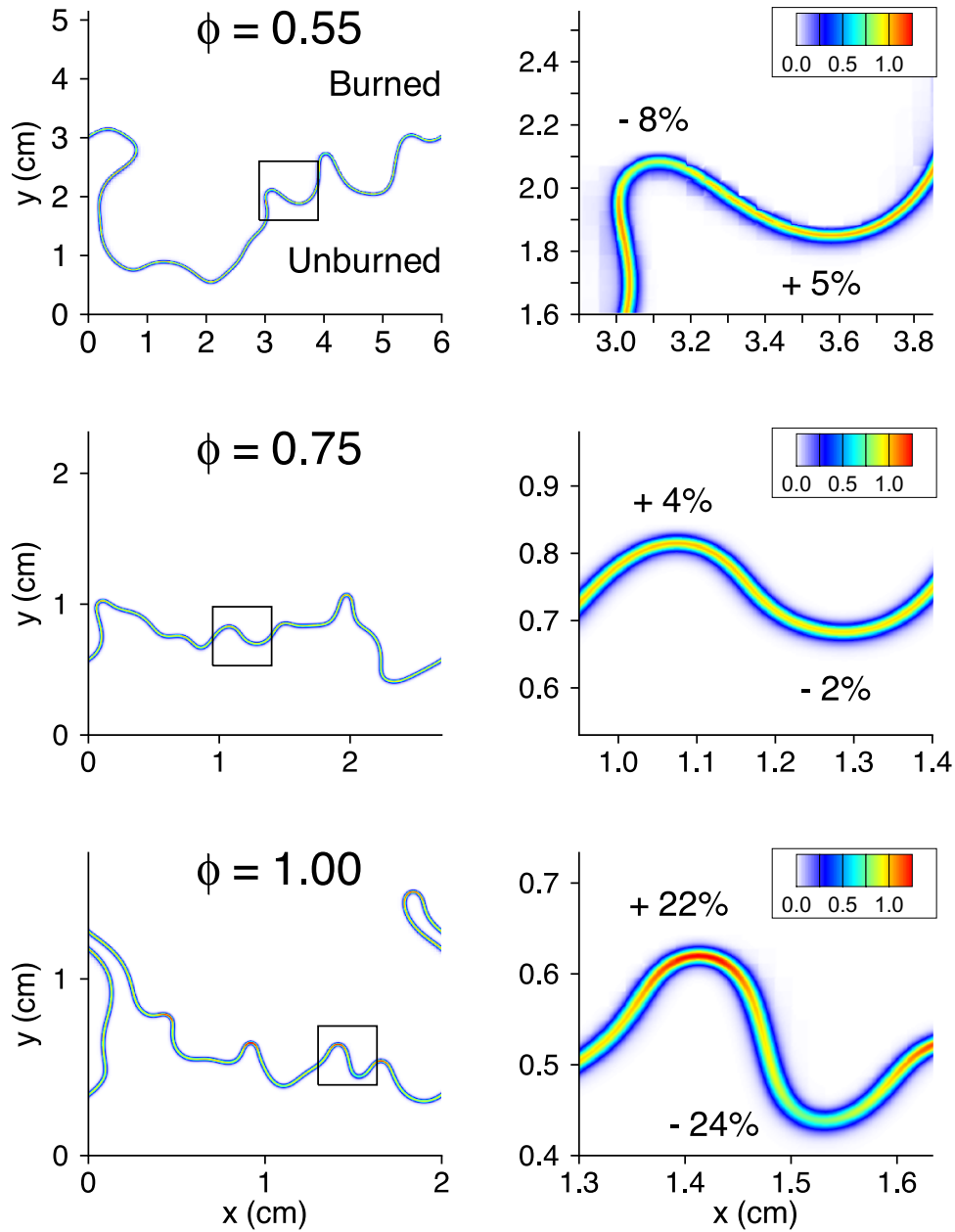


Figure 10: Fuel consumption is often used as a measure of local flame speed. This figure depicts the ratio of local methane consumption to peak consumption in unstretched laminar flames of identical fuel equivalence ratios. Reference values are given in Table 1.

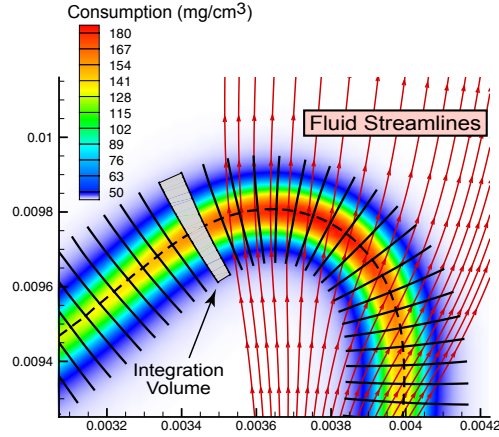


Figure 11: *Construction of local control volumes at a typical flame surface. The volumes are centered on the flame, and extend normal to the local isopleths in progress variable at uniform intervals along the flame. Adjacent flame normals define a volume over which we define the local consumption-based burning speed.*

these integrals are relatively easy to evaluate accurately and provide a fairly robust characterization of the local burning. Evaluation of the intersected area,  $A^{\ell,i}$ , is sensitive to the definition of the flame surface (in this case, the choice of progress variable and of its isocontour) which can introduce a small bias into the curvature correlation. In the present cases, however, the fuel consumption profile takes on non-negligible values over a relatively limited range in temperature, so we can minimize this bias by ensuring the flame isotherm is centered near this narrow peak. The values chosen in Table 1 correspond to the peak in heat release for the corresponding steady flat flame solution.

The data in Figure 10 shows a clear dependence of the local fuel consumption on the local flame curvature. To make the notion more precise, we form the consumption-based local flame speed  $S_c^\ell$  at each segment along the flame as discussed above and form scatter plots, shown in Figure 12, of the local flame speed normalized by the laminar flame speed with the curvature normalized by thermal flame thickness. The scatter plots confirm the trend shown in Figure 10, namely, that the  $\phi = 1.0$  flame correlates negatively with curvature while the  $\phi = 0.55$  flame correlates positively. In addition, the relative insensitivity of the  $\phi = 0.75$  flame is apparent. If we associate a curvature Markstein number,  $\mathcal{M}_\kappa$ , with the slope of the correlation for each case in Figure 12, then the data matches the trend reported in [39], including the change of sign of the Markstein number near  $\phi = 0.75$ . The magnitude of the Markstein number is sensitive to the definitions of flame thickness, burning speed, flame isopleth, etc. For this reason, it is difficult in general to make detailed quantitative comparisons with the results from other numerical and experimental studies.

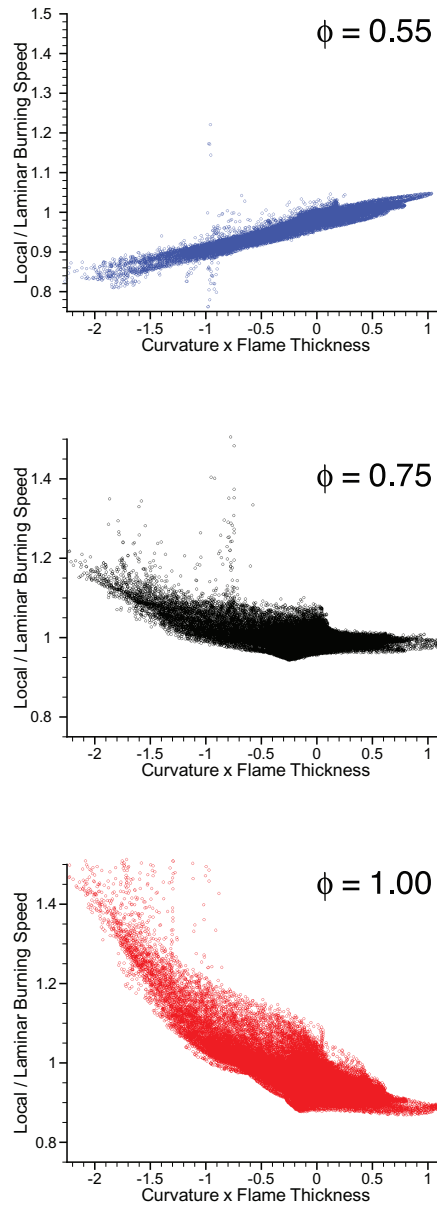


Figure 12: *Scatter plot of local turbulent flame speed scaled by laminar flame speed versus of curvature scaled by laminar flame thickness, for the three flames of different stoichiometries.*

Each of the scatter plots shows a number of outlier points, most notably around normalized curvature of  $-1$ . To explain this phenomena, we note that in rare situations the regions used to define the integrated local flame speed can

become overly distorted or poorly defined. These correspond to regions where an elongated cusp closes, or when the sides of an elongated cusp burn together and change the local topology of the flame. In both cases, an ambiguity in definition of the wedge-shaped regions develops approximately when the flame thickness is equal to the local radius of curvature, that is, where the magnitude of the normalized curvature is unity.

From wrinkled flame theory, as explained for example by Peters [28] and Poinsoot and Veynante [29], we expect the local flame speed to correlate with stretch, which combines the effects of curvature,  $\kappa$ , and strain tangential to the flame surface,  $\mathcal{S}_t = \hat{t} \cdot \nabla \vec{v} \cdot \hat{t}$ , where  $\hat{t} \perp \hat{n}$  is the unit vector locally tangent to the flame. The evaluation of stretch in an idealized setting of an “infinitely” thin flame propagating through a fluid is fairly straightforward. In the present setting, where the flame is being resolved and has a finite thickness, it is unclear how to evaluate the strain term in the definition of stretch. There is a large literature on the generalization of classical flame theory to “thick” flames, see [11, 16–18] and references therein. We pursued several possible approaches to computing stretch; however, local definitions of the stretch appear to be highly sensitive to the method of evaluating the strain rate. Furthermore, for the approaches we considered, the effects of strain on speed-versus-stretch correlations were entirely explained by the correlation of strain with curvature. A similar observation was made by Haworth and Poinsoot [20]. Pope [31] also discusses the interrelationship of curvature and strain. Consequently, at least for the flames considered here, the variation in consumption speed along the flame is essentially a function of curvature alone. The difficulties with defining a local strain rate for the definition of stretch suggests that an integral-based approach, as for example [18, 25], is needed to obtain a more robust and physically meaningful method for computing stretch.

## 5 Conclusions

We have introduced a new computational tool based on applying a feedback mechanism to control and stabilize a turbulent flame in a simple two dimension geometry without introducing a geometric stabilization mechanism such as a flow obstruction or a stagnation plate. We have used this tool to study the behavior of premixed turbulent methane flames in two dimensions. For these simulations we examined both the global flame behavior and the dependence of the local flame speed on flame curvature. By using the control algorithm, we are able to hold the flame at conditions that are statistically stationary, enabling us to obtain detailed diagnostics for an ensemble of snapshots of the flame at the same turbulent conditions. In future work, we will present a more detailed analysis of local flame dynamics and flame chemistry. In addition, the methodology presented here extends in a straightforward fashion to three dimensions. Applications to three-dimensional turbulent flames will also be presented in future work.

## Acknowledgments

The authors would like to thank Jonathan Goodman and Alan Laub for helpful discussions in the course of this work. This research used resources of the National Center for Computational Sciences at Oak Ridge National Laboratory, which is supported by the Office of Science of the U.S. Department of Energy under Contract No. DE-AC05-00OR22725. The authors were supported by the Office of Science through the Office of Advanced Scientific Computing Research, Mathematical, Information, and Computational Sciences Division under U.S. Department of Energy contract DE-AC03-76SF00098.

## References

- [1] A. S. Almgren, J. B. Bell, P. Colella, L. H. Howell, and M. L. Welcome. A conservative adaptive projection method for the variable density incompressible Navier-Stokes equations. *J. Comput. Phys.*, 142:1–46, May 1998.
- [2] M. Baum, T. J. Poinso, D. C. Haworth, and N. Darabiha. Direct numerical simulation of  $\text{H}_2/\text{O}_2/\text{N}_2$  flames with complex chemistry in two-dimensional turbulent flows. *J. Fluid Mech.*, 281:1–32, 1994.
- [3] J. B. Bell, M. S. Day, and J. F. Grcar. Numerical simulation of premixed turbulent methane combustion. *Proc. Combust. Inst.*, 29:1987–1993, 2002.
- [4] J. B. Bell, M. S. Day, I. G. Shepherd, M. Johnson, R. K. Cheng, J. F. Grcar, V. E. Beckner, and M. J. Lijewski. Numerical simulation of a laboratory-scale turbulent V-flame. *Proc. Natl. Acad. Sci. USA*, 102(29):10006–10011, 2005.
- [5] D. Bradley. How fast can we burn? *Proc. Combust. Inst.*, 24:247–262, 1992.
- [6] P. E. Caines. *Linear Stochastic Systems*. John Wiley, New York, 1988.
- [7] N. Chakraborty and S. Cant. Unsteady effects of strain rate and curvature on turbulent premixed flames in an inflow outflow configuration. *Combust. Flame*, 137:129–147, 2004.
- [8] G. Chen, G. Chen, and S.-H. Hsu. *Linear Stochastic Control Systems*. CRC Press, Boca Raton, 1995.
- [9] Y.-C. Chen, P. A. M. Kalt, R. W. Bilger, and N. Swaminathan. Effects of mean flow divergence on turbulent scalar flux and local flame structure in premixed turbulent combustion. *Proc. Combust. Inst.*, pages 1863–1871, 2002.
- [10] R. K. Cheng and I. G. Shepherd. The influence of burner geometry on premixed turbulent flame propagation. *Combust. Flame*, 85:7–26, 1991.

- [11] S. H. Chung and C. K. Law. An integral analysis of the structure and propagation of stretched premixed flames. *Combust. Flame*, 72:325–336, 1988.
- [12] O. Colin, F. Ducros, D. Veynante, and T. Poinso. A thickened flame model for large eddy simulations of turbulent premixed combustion. *Phys. Fluids*, 12(7):1843–1863, 2000.
- [13] M. S. Day and J. B. Bell. Numerical simulation of laminar reacting flows with complex chemistry. *Combust. Theory Modelling*, 4:535–556, 2000.
- [14] F. L. Dryer and I. Glassman. High-temperature oxidation of CO and CH<sub>4</sub>. *Proc. Combust. Inst.*, 14:987–1003, 1972.
- [15] M. Frenklach, H. Wang, M. Goldenberg, G. P. Smith, D. M. Golden, C. T. Bowman, R. K. Hanson, W. C. Gardiner, and V. Lissianski. GRI-Mech—an optimized detailed chemical reaction mechanism for methane combustion. Technical Report GRI-95/0058, Gas Research Institute, 1995. [http://www.me.berkeley.edu/gri\\_mech/](http://www.me.berkeley.edu/gri_mech/).
- [16] L. P. H. de Goey, R. M. M. Mallens, and J. H. M. ten Thijsse Boonkcamp. An evaluation of different contributions to flame stretch for stationary premixed flames. *Combust. Flame*, 110:54–66, 1997.
- [17] L. P. H. de Goey and J. H. M. ten Thijsse Boonkcamp. A mass-based definition of flame stretch for flames with fine thickness. *Combustion Science and Technology*, 122:399–405, 1997.
- [18] L. P. H. de Goey and J. H. M. ten Thijsse Boonkcamp. A flamelet description of premixed laminar flames and the relation with flame stretch. *Combust. Flame*, 119:253–271, 1999.
- [19] D. C. Haworth, R. J. Blint, B. Cuenot, and T. J. Poinso. Numerical simulation of turbulent propane-air combustion with nonhomogeneous reactants. *Combust. Flame*, 121:395–417, 2000.
- [20] D. C. Haworth and T. J. Poinso. Numerical simulations of Lewis number effects in turbulent premixed flames. *J. Fluid Mech.*, 244:405–436, 1992.
- [21] J. O. Hinze. *Turbulence*. McGraw-Hill, 2 edition, 1975.
- [22] R. J. Kee, J. F. Grcar, M. D. Smooke, and J. A. Miller. PREMIX: A fortran program for modeling steady, laminar, one-dimensional premixed flames. Technical Report SAND85-8240, Sandia National Laboratories, Livermore, 1983.
- [23] H. Kushner. *Introduction to Stochastic Control*. Holt, Rinehart and Winston, New York, 1971.

- [24] D. Most, F. Dinkelacker, and A. Leipertz. Lifted reaction zones in premixed turbulent bluff-body stabilized flames. *Proc. Combust. Inst.*, 29:1801–1806, 2002.
- [25] J. A. van Oijen, G. R. A. Groot, R. J. M. Bastiaans, and L. P. H. de Goeij. A flamelet analysis of the burning velocity of premixed turbulent expanding flames. *Proc. Combust. Inst.*, 30(1):657–664, 2005.
- [26] R. B. Pember, L. H. Howell, J. B. Bell, P. Colella, W. Y. Crutchfield, W. A. Fiveland, and J. P. Jessee. An adaptive projection method for unsteady, low-Mach number combustion. *Combust. Sci. Technol.*, 140:123–168, 1998.
- [27] N. Peters. Laminar flamelet concepts in turbulent combustion. *Proc. Combust. Inst.*, 21:1231–1250, 1986.
- [28] N. Peters. *Turbulent Combustion*. Cambridge University Press, Cambridge, 2000.
- [29] T. Poinso and D. Veynante. *Theoretical and Numerical Combustion*. R. T. Edwards, Inc., Philadelphia, 2001.
- [30] T. Poinso, D. Veynante, and S. Candel. Diagrams of premixed turbulent combustion based on direct simulation. *Proc. Combust. Inst.*, 23:613–619, 1990.
- [31] S. B. Pope. The evolution of surfaces in turbulence. *Int. J. Engng. Sci.*, 26:445–469, 1988.
- [32] C. J. Rutland and A. Trouvé. Direct simulations of premixed turbulent flames with non-unit Lewis numbers. *Combust. Flame*, 94:41–57, 1993.
- [33] S. S. Sattler, D. A. Knaus, and F. C. Gouldin. Determination of three-dimensional flamelet orientation distributions in turbulent V-flames from two-dimensional image data. *Proc. Combust. Inst.*, 29:1785–1795, 2002.
- [34] I. G. Shepherd, R. K. Cheng, T. Plessing, C. Kortschik, and N. Peters. Premixed flame front structure in intense turbulence. *Proc. Combust. Inst.*, 29:1833–1840, 2002.
- [35] G. P. Smith, D. M. Golden, M. Frenklach, N. W. Moriarty, B. Eiteneer, M. Goldenberg, C. T. Bowman, R. K. Hanson, S. Song, W. C. Gardiner Jr., V. V. Lissianski, and Z. Qin. GRI-Mech 3.0. [http://www.me.berkeley.edu/gri\\_mech/](http://www.me.berkeley.edu/gri_mech/).
- [36] M. Tanahashi, M. Fujimura, and T. Miyauchi. Coherent fine scale eddies in turbulent premixed flames. *Proc. Combust. Inst.*, 28:529–535, 2000.
- [37] M. Tanahashi, Y. Nada, Y. Ito, and T. Miyauchi. Local flame structure in the well-stirred reactor regime. *Proc. Combust. Inst.*, 29:2041–2049, 2002.

- [38] A. Trouvé and T. J. Poinso. The evolution equation for the flame surface density in turbulent premixed combustion. *J. Fluid Mech.*, 278:1–31, 1994.
- [39] L.-K. Tseng, M. A. Ismail, and G. M. Faeth. Laminar burning velocities and Markstein numbers of hydrocarbon / air flames. *Combust. Flame*, 95:410–425, 1993.
- [40] C. K. Westbrook and F. L. Dryer. Simplified reaction mechanisms for the oxidation of hydrocarbon fuels in flames. *Combust. Sci. Technol.*, 27:31–43, 1981.
- [41] S. Zhang and C. J. Rutland. Premixed flame effects on turbulence and pressure-related terms. *Combust. Flame*, 102:447–461, 1995.
- [42] V. L. Zimont and Y. M. Trushin. Total combustion kinetics of hydrocarbon fuels. *Comb. Expl. Shock Wave*, 5:391–194, 1969.



**List of Figures**

1	Synthetic flame control simulations – flame location. . . . .	7
2	Synthetic flame control simulations – control velocity. . . . .	7
3	Synthetic flame control simulations starting from correct flame location and speed. . . . .	8
4	Performance of control algorithm for $\phi = 1.0$ case with simplified chemistry. . . . .	10
5	Temperature in the three flames. . . . .	12
6	Probability density of curvature scaled by laminar flame thickness for the three flames of different stoichiometries. Density is calculated by a moving average over 5 intervals of width 0.02 (nondimensional) on the horizontal axis. . . . .	13
7	Turbulent flame speed for the three flames. . . . .	14
8	Probability density of overall turbulent speedup for the three flames of different stoichiometries. Density is calculated by a moving average over 5 intervals of width 0.05 (nondimensional) on the horizontal axis. . . . .	15
9	Turbulent flame speed versus flame area. . . . .	15
10	Fuel consumption is often used as a measure of local flame speed. This figure depicts the ratio of local methane consumption to peak consumption in unstretched laminar flames of identical fuel equivalence ratios. Reference values are given in Table 1. . . . .	17
11	Construction of local control volumes at a typical flame surface. The volumes are centered on the flame, and extend normal to the local isopleths in progress variable at uniform intervals along the flame. Adjacent flame normals define a volume over which we define the local consumption-based burning speed. . . . .	18
12	Scatter plot of local turbulent flame speed scaled by laminar flame speed versus of curvature scaled by laminar flame thickness, for the three flames of different stoichiometries. . . . .	19

---

## Disclaimer

This document was prepared as an account of work sponsored by the United States Government. While this document is believed to contain correct information, neither the United States Government nor any agency thereof, nor The Regents of the University of California, nor any of their employees, makes any warranty, express or implied, or assumes any legal responsibility for the accuracy, completeness, or usefulness of any information, apparatus, product, or process disclosed, or represents that its use would not infringe privately owned rights. Reference herein to any specific commercial product, process, or service by its trade name, trademark, manufacturer, or otherwise, does not necessarily constitute or imply its endorsement, recommendation, or favoring by the United States Government or any agency thereof, or The Regents of the University of California. The views and opinions of authors expressed herein do not necessarily state or reflect those of the United States Government or any agency thereof, or The Regents of the University of California.

Ernest Orlando Lawrence Berkeley National Laboratory is an equal opportunity employer.

---